

SEARCH FOR LONG-TERM REENTRY DISPOSAL ORBITS ACROSS ALTITUDE AND INCLINATION

Alan B Jenkin⁽¹⁾, John P. McVey⁽²⁾, Marlon E. Sorge⁽³⁾, Glenn E. Peterson⁽⁴⁾

(1) The Aerospace Corporation, P.O. Box 92957, Los Angeles, CA 90009-2957, USA, Email:

Alan.B.Jenkin@aero.org

(2) The Aerospace Corporation, P.O. Box 92957, Los Angeles, CA 90009-2957, USA, Email:

John.P.McVey@aero.org

(3) The Aerospace Corporation, 2155 Louisiana Blvd., NE, Suite 5000, Albuquerque, NM 87110-5425, USA,

Email: Marlon.E.Sorge@aero.org

(4) The Aerospace Corporation, P.O. Box 92957, Los Angeles, CA 90009-2957, USA, Email:

Glenn.E.Peterson@aero.org

ABSTRACT

The 2019 U.S. Government Orbital Debris Mitigation Standard Practices [1] contain a new disposal option for long-term reentry within 200 years. This option allows spacecraft operating above low Earth orbit (LEO) to use eccentricity growth due to natural orbital perturbations for eventual reentry of a spacecraft. An analysis was performed to determine the range of disposal orbit altitude and inclination above LEO that could potentially use this new disposal option. The study also assessed the long-term collision probability for these disposal orbits. Results show that orbital lifetime less than 200 years can be achieved for an inclination region above 50° and a broad altitude region starting near the Global Navigation Satellite Systems that extends upward and includes inclined geosynchronous orbits. Collision probability is lowest in the inclination/altitude range where orbital lifetime is less than 200 years, or in the low inclination range below 20° and high-altitude range above 47,000 km, where disposal orbits are stable and the background population is sparse.

1 INTRODUCTION

The 2019 U.S. Government Orbital Debris Mitigation Standard Practices [1] contain a new disposal option for long-term reentry within 200 years. This option allows use of eccentricity growth due to natural orbital perturbations for eventual reentry of a spacecraft. It is intended primarily for spacecraft operating above low Earth orbit (LEO). Spacecraft operating in LEO would still be subject to the 25-year lifetime rule. The new option serves as an alternative to using permanent disposal orbits and is beneficial for orbital debris mitigation above LEO. The study of [2] (see Fig. 24) showed that, for near-circular inclined geosynchronous orbits (IGSOs), use of long-term reentry reduces collision risk by almost two orders-of-magnitude compared to the collision risk for traditional low inclination geosynchronous (GEO) storage disposal orbits, with no

increase in disposal delta-V cost. The study of [3] showed that constraints on time spent by a disposed spacecraft in the LEO, GEO and semi-synchronous zones in the 2019 ODMSP (conditions for using the long-term reentry option) can be met by near-circular IGSOs, eccentric IGSOs (e.g., Tundra orbits), and GPS disposal orbits.

Numerous extensive studies have been performed in recent years on the use of natural orbital perturbations to achieve eventual reentry. The studies of [2, 4-6] considered the orbital region near GEO. The study of [6] compared disposal options for Tundra orbits and showed that long-term reentry is by far the most cost-effective in terms of delta-V and collision risk reduction. The studies of [7-8] considered medium Earth orbit (MEO) and geosynchronous transfer orbits (GTOs). [9] presented software for assessing disposal options for LEO, MEO, GTO, and GEO missions, including long-term reentry.

In the study presented here, an analysis was performed to determine the range of disposal orbit altitude and inclination above LEO that could potentially use this new disposal option. The study also presents an assessment of the long-term collision probability for these disposal orbits.

2 ORBITAL RESONANCES

Orbital resonances play a key role in eccentricity growth and the reentry of disposal orbits above LEO. These resonances occur when the orbit of the satellite has a rotation that synchronizes with the rotation of the apparent orbit of the Sun or Moon relative to the Earth. Mathematically this occurs when the integer combination of the rates of the spacecraft orbit right ascension of ascending node (RAAN = Ω), argument of perigee (AOP = ω_p), and the RAAN of the 3rd body (Sun or Moon, Ω_j) apparent orbit relative to the Earth sum to zero, as expressed in this equation.

$$n\dot{\omega}_p + m\dot{\Omega} - l\dot{\Omega}_j = 0 \quad (1)$$

where n , m , and l are integers.

George Chao derived the doubly averaged equation for variation of eccentricity (e) due to third-body gravitational perturbations (from Eq. 6.9 in [10], Eq. 5.9 in [11]).

$$\frac{de}{dt} = -\sum_{j=1}^2 \left(\frac{15}{8}\right) e \gamma_j s \left[c_1 \sin(2(\omega_p - \Delta\Omega_j)) + c_2 \sin(2\omega_p - \Delta\Omega_j) + c_3 \sin(2\omega_p) + c_4 \sin(2\omega_p + \Delta\Omega_j) + c_5 \sin(2(\omega_p + \Delta\Omega_j)) \right] \quad (2)$$

The summation is performed over the two perturbing bodies ($j=1$ is for the Sun, $j=2$ is for the Moon). The coefficients c_k are analytical functions of the orbit inclinations of both the vehicle orbit and the third-body orbit relative to the equator. $\Delta\Omega$ is the difference between the RAANs of the vehicle orbit and the third-body orbit relative to the Earth's equator ($\Delta\Omega = \Omega - \Omega_j$). See [10, 11] for formulas for the coefficients c_k and the factors γ_j and s . This expression is derived via computerized series expansion of the third-body disturbing potential (Eq. 3.8 in [11]) in terms of the ratio of the spacecraft radial distance from the Earth center to the radial distance of the third body from the Earth center. It assumes that the apparent orbits of the Sun and Moon are circular. Note that sine terms with arguments containing values of m and n (see Eq. 1) larger than 2 are higher order terms in the expansion and are not dominant.

From Eqs. 1 and 2, it turns out that there are five resonance angles, corresponding to the five coefficients in Eq. 2, that dominate the evolution of orbits.

$$c_1: \alpha_1 = \omega_p - \Omega \quad (3)$$

$$c_2: \alpha_2 = \omega_p - \frac{1}{2}\Omega \quad (4)$$

$$c_3: \alpha_3 = \omega_p \quad (5)$$

$$c_4: \alpha_4 = \omega_p + \frac{1}{2}\Omega \quad (6)$$

$$c_5: \alpha_5 = \omega_p + \Omega \quad (7)$$

Both Ω and ω , and therefore the resonance angles, are functions of spacecraft orbit inclination, semimajor axis, and eccentricity through the effect of Earth gravity and Sun and Moon gravity on the rates $\dot{\Omega}$ and $\dot{\omega}_p$. The long-term resonance with the apparent Sun orbit occurs when the resonance angle rates $\dot{\alpha}_k$ equal zero. In this paper, these resonance conditions are referred to by the corresponding coefficient in Eq. 2.

The rates $\dot{\Omega}$ and $\dot{\omega}_p$ determined by the first-order J_2 term of Earth gravity field harmonic expansion are given by Eqs. 8 and 9 (from Eqs. 8-37 and 8-39 in [12]).

$$\dot{\Omega} = -\frac{3nR_E^2 J_2}{2p^2} \cos(i) \quad (8)$$

$$\dot{\omega}_p = \frac{3nR_E^2 J_2}{2p^2} \left[2 - \frac{5}{2} \sin^2(i) \right] \quad (9)$$

where n is the spacecraft orbit mean motion, $p = a(1 - e^2)$ is the semi-latus rectum, a is the semi-major axis (SMA), and R_E is the mean equatorial radius of the Earth.

Fig. 1 shows the variation of the angle rates with inclination as determined by Eqs 3-9. The example presented is for a near-circular GEO orbit. As can be seen from the plot, there are distinct inclinations where the rates for different resonance conditions are zero. Five conditions of resonance with the Sun apparent orbit occur at the following inclinations: 73.1° (c_1), 69° (c_2), 63.4° (c_3), 56° (c_4), and 46.4° (c_5). These values of inclination are mirrored in the inclination range from 90° to 180° . Eqs. 3-9 indicate that these inclinations corresponding to zero resonance angle rates (due to J_2 only) do not vary with altitude. Note from the figure that for this orbit none of the resonance angle rates is high enough to match the mean nodal regression rate of the apparent orbit of the Moon.

When the resonance angle rates are zero, the line of apsides follows a motion relative to the plane of the apparent Sun orbit that repeats over time. This repeated motion determines how the effect of Sun gravity on the spacecraft orbit accumulates over time. Fig.2 illustrates the repeated path traced out by the apogee point of an eccentric IGSO relative to the plane of the apparent Sun orbit for the c_3 resonance condition. The spacecraft orbit is magenta, the path of the apogee point is orange, the line to the Sun is yellow, and the plane of the apparent Sun orbit is represented by the blue grid. The path of the apogee point is invariant with initial RAAN. Fig. 3 shows the corresponding illustration for the c_4 resonance condition when initial RAAN = 180° . The non-symmetric spread of the apogee path in 3D space results in a net accumulation of the effect of Sun gravity on the orbital eccentricity.

As altitude increases, the inclination variation with time due to Sun and Moon gravity increases and eventually becomes large enough to cause these resonances to overlap with each other.

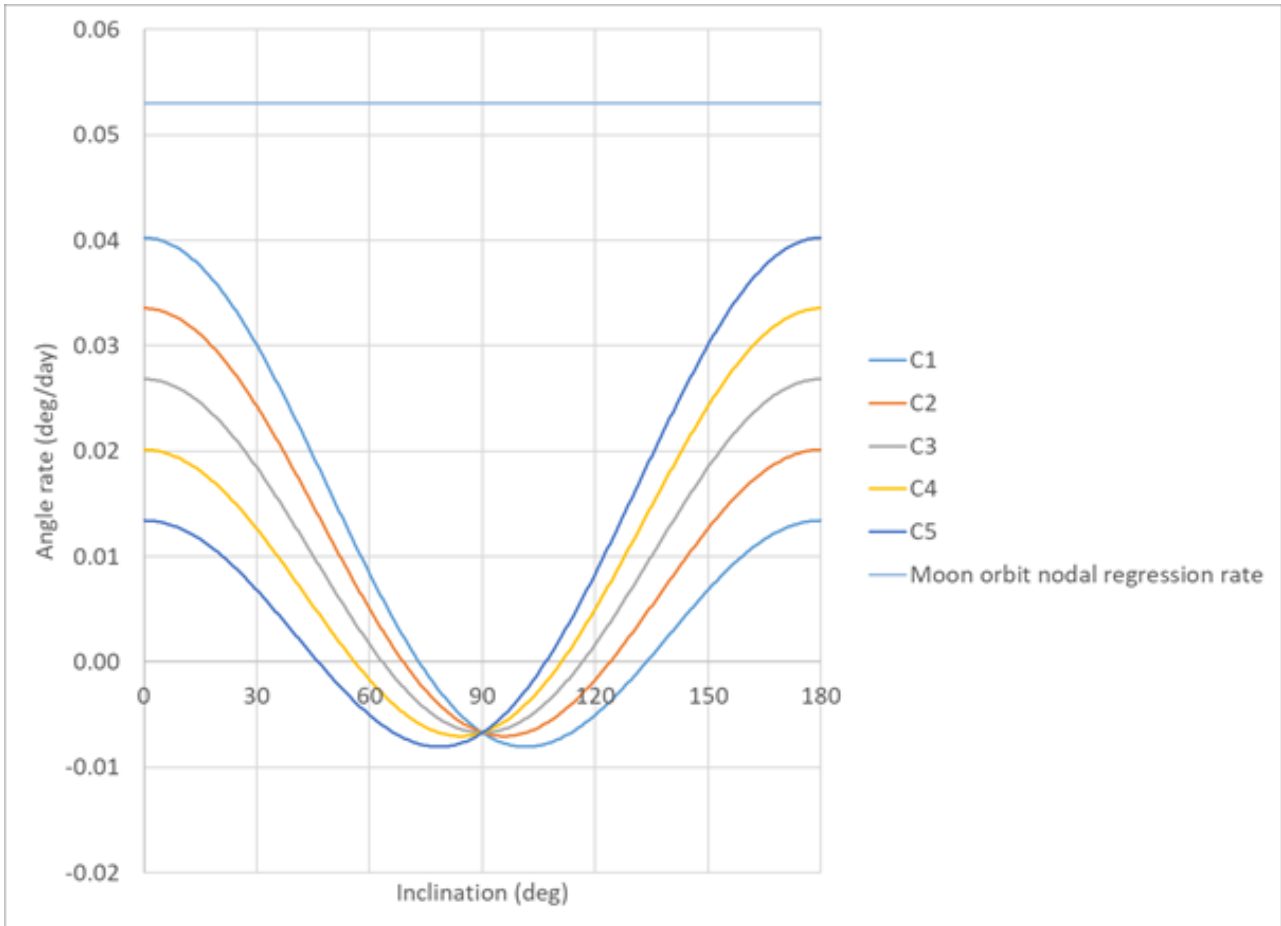


Figure 1. Plot of the five resonance angle rates vs. inclination for a near-circular geosynchronous orbit, as determined by the J_2 component of Earth gravity field only.

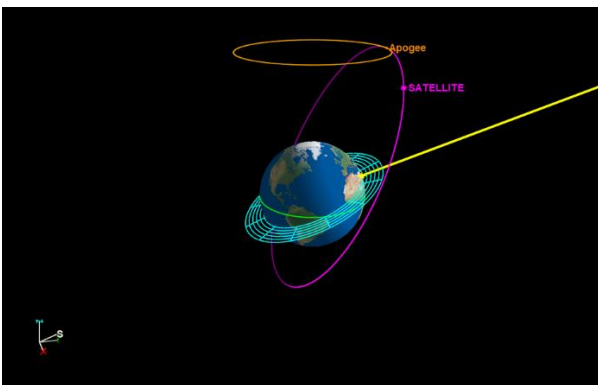


Figure 2. Illustration of the repeated path (orange) traced out by the apogee point of an eccentric (0.268) IGSO for the c_3 resonance condition (rendered with Satellite Orbit Analysis Program).

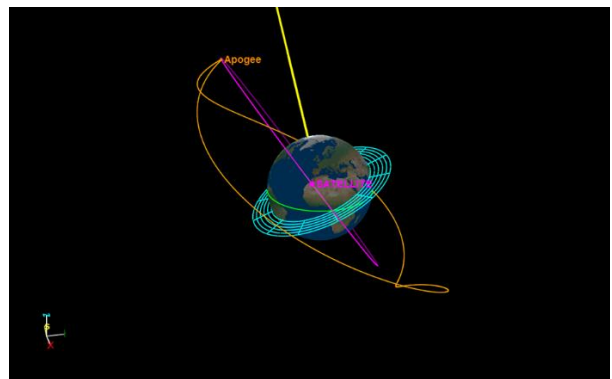


Figure 3. Illustration of the repeated path (orange) traced out by the apogee point of an eccentric (0.268) IGSO for the c_4 resonance condition when initial RAAN = 180° (rendered with Satellite Orbit Analysis Program).

3 LIDOV-KOZAI MECHANISM

The Lidov-Kozai mechanism also plays an important role in reentry of disposal orbits above LEO. In 1962, Mikhail

Lidov [13] presented an analytical determination of the orbital evolution of a satellite about a planet, e.g., the Earth, under the gravitational perturbation of a distant third body, e.g., the Moon. His derivation showed that the projected component of the angular momentum of the satellite orbit into the direction of the normal vector of the orbital plane of the third body is constant, and the consequence of that is that the eccentricity and inclination are coupled and vary inversely. Shortly afterward, Yoshihide Kozai [14] performed an analysis of orbital evolution of a satellite, in this case a comet, about a central body, in this case the Sun, under the gravitational perturbation of a distant third body, in this case Jupiter. Kozai cited Lidov's paper. In Kozai's paper, Table 1 and Fig. 1 show a critical inclination above which eccentricity-inclination oscillation can occur as a function of the ratio of the satellite orbital radius to the perturbing body apparent orbital radius. For example, at an altitude of 100,000 km, the critical inclination relative to the apparent orbit of the Sun is approximately 39° . The critical inclination relative to the apparent orbit of the Moon is approximately 35° .

These theories have the following limitations: they do not account for non-uniform mass distribution in the Earth, and they assume there is only one third perturbing body, so only the Sun or the Moon.

More recently, in 2016, a theory similar to that of Kozai but also including the Earth oblateness term was developed by Gkolias, Daquin, Gachet, and Rosengren [15] to study the chaos in orbital evolution over long periods of time. Similar to the Kozai theory, they used a Hamiltonian perturbation theory. They considered the altitude range from 3 to 7 Earth radii, going from approximately 19,000 km to 45,000 km altitude. They performed propagations over 465 years. Their results presented in [15] include plots of normalized maximum eccentricity over the propagation time period vs. initial semimajor axis and inclination, similar to what is shown in the work presented here. Their results showed resonance inclination regions widening and overlapping as the semimajor axis increases, and over sufficiently long periods of time, the inclination moves from one resonance to another, leading to chaotic orbital evolution.

4 STUDY METHODOLOGY

In this study, a slightly eccentric disposal orbit was selected as a reference case for a parametric variation. The initial SMA altitude ($a - R_E$) was varied from 2,000 km, the upper bound of LEO, up to 100,000 km, which is approx. $\frac{1}{4}$ the distance to the Moon, at increments of 1,000 km. The inclination was varied from 0° to 90° at 1° increments. The initial eccentricity was selected to be 0.02. This can be achieved for a reasonable delta-V from a mission orbit with eccentricity of 0.003 or less. This level of initial eccentricity facilitates more accurate targeting of AOP, thereby helping to reduce the orbital

lifetime. Regarding the RAAN, four values were considered: 0° , 90° , 180° , and 270° . AOP was set to 270° , following previous studies by the authors [2, 6]. It is noted that there are other values that could result in more eccentricity growth, depending upon the inclination (e.g., resonance condition) and RAAN, but these were not considered in this study. The epoch was selected to be August 26, 2018, midnight UTC, to be consistent with previous studies by the authors [2, 6]. A generic spacecraft was selected with a mass of 2000 kg and cross-sectional area for solar radiation pressure and drag forces of 20 m^2 . These values are not representative of any specific actual satellite. With this type of mass and area, the area-to-mass ratio causes the solar radiation pressure to be a very small player in the long-term evolution of the disposal orbit.

5 LONG-TERM PROPAGATION ANALYSIS

The precision integration code TRACE was used to propagate the disposal orbits. The use of this code for the orbit element sweeps was made possible by the availability of cluster computing. The force model settings were as follows:

- 70 x 70 modified EGM-96 Earth gravity model.
- Sun and Moon gravity.
- Solar radiation pressure, with an assumed reflectivity coefficient of 1.3.
- Regularized time.
- NRLMSISE-00 atmosphere model, with an assumed drag coefficient of 2.2.
- Used monthly predictions of 50-percentile level of solar flux ($F_{10.7}$) and geomagnetic index (A_p) from December 2017 to 2030 from NASA Marshall Space Flight Center (MSFC, based on NOAA data) for the propagation. For years after 2030, the last 11-years of MSFC predicted data were repeated into the future.
- Reentry altitude: 120 km.

Propagation was performed until reentry or a maximum time period of 200 years had elapsed. These runs were executed on the Aerospace computing cluster.

Fig. 4 shows the results of the long-term orbit propagation. This 3D surface plot shows maximum eccentricity over 200 years on the z-axis and the color bar as a function of the initial inclination and altitude of the disposal orbit for initial RAAN = 180° . The flat top of the surface indicates reentry occurring within 200 years. From the surface plot, it is seen that the c_3 and c_4 resonances are distinct in the lower altitude range, but as altitude increases they blur together. The c_1 and c_2 resonances are not easily visible. At low inclination, there is another resonance, which may be the c_5 resonance

occurring at a lower inclination as altitude increases due to increasing effect of Sun and Moon gravity perturbations. From the plot it is seen that, as altitude increases, there is a broad range of inclination and

altitude that has high eccentricity growth and achieves reentry within 200 years. It is also seen that there is a boundary where eccentricity growth starts, similar to the critical inclination value in the Lidov-Kozai theory.

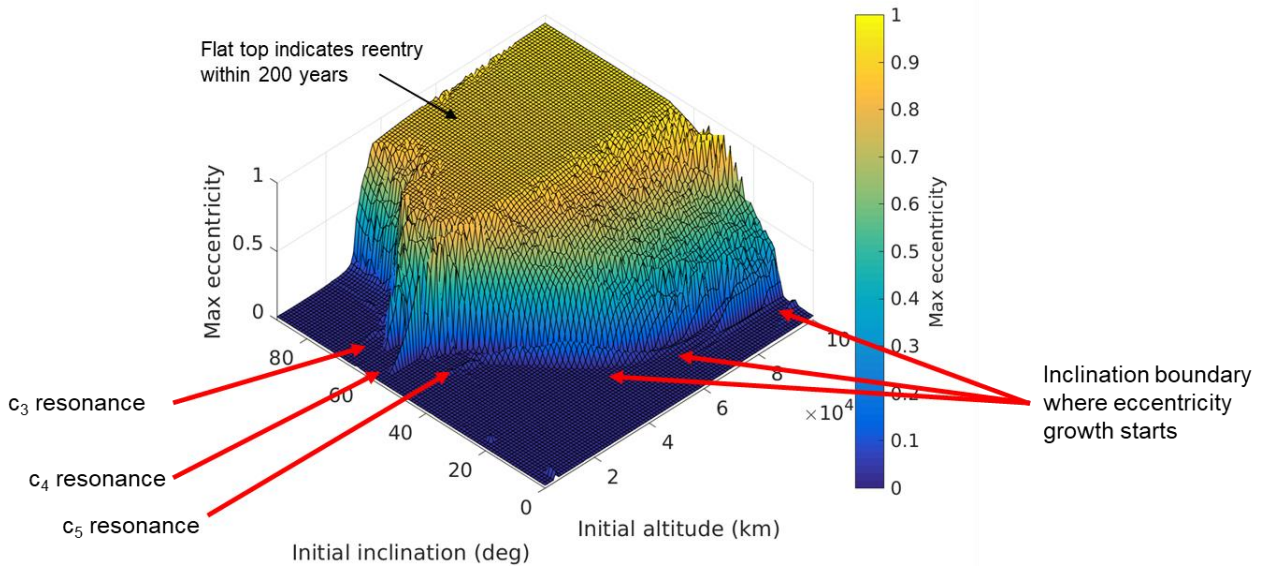


Figure 4. 3D Plot of maximum eccentricity over 200 years vs. initial altitude and inclination, initial RAAN = 180°.

Fig. 5 shows together in one panel the plots for all four initial RAAN values considered in the study here. From this plot, we see that the region of high eccentricity growth varies significantly between the four initial RAAN values, with the initial RAAN value of 180° having the largest region of reentry within 200 years. We also see that the four plots become more differentiated as altitude increases. This variation with initial RAAN may be a reflection of the variation of the orientation of the Laplace plane with altitude. The Laplace plane is the plane with a normal axis about which the spacecraft orbital plane precesses with minimal change in relative inclination [16]. At lower altitude, the orientation of the

Laplace plane will be closer to that of the equator of the Earth. At GEO, the Laplace plane has a RAAN of approximately 0° and inclination of approximately 7.3°. Therefore, there is a 14.6° (= 2 x 7.3°) variation with RAAN of the inclination boundary where orbital eccentricity growth starts. At higher altitude, the orientation of the Laplace plane will approach the plane of the apparent orbit of the third body about the Earth, in this case presumably the Sun with an apparent orbit inclination of 23.5°. This would result in a 47° (= 2 x 23.5°) variation with RAAN of the inclination boundary where orbital eccentricity growth starts.

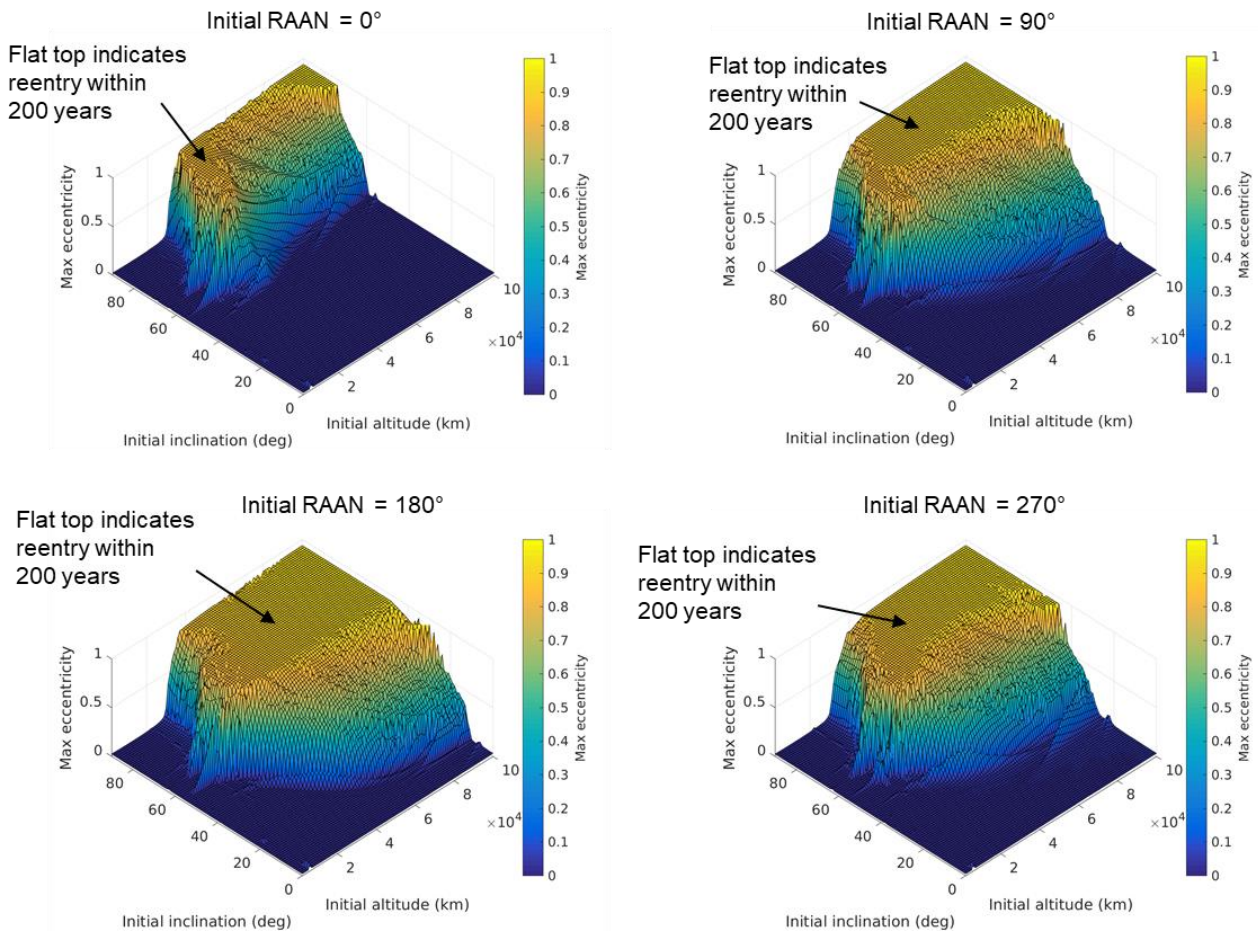


Figure 5. 3D Plots of maximum eccentricity over 200 years vs. initial altitude and inclination, initial RAAN = 0° , 90° , 180° , and 270° .

Fig. 6 is a 2D version of Fig. 4. Overlaid on this plot are the various resonance conditions c_1 to c_5 , as well as the various Global Navigation Satellite Systems (GNSS), and a vertical line representing the altitude at GEO. The plot is similar to Fig. 5 in the study by Gkolias et al. [15]. From this plot we see that the GNSS are near c_3 and c_4 resonances in a region where they are still distinct. GEO

on the other hand is at a higher altitude where the resonances are no longer distinct. GEO has a broad inclination range of high eccentricity growth. Finally, we see here the apparent c_5 resonance with the inclination being modified as the altitude increases due to increasing effect of Sun and Moon gravity perturbations.

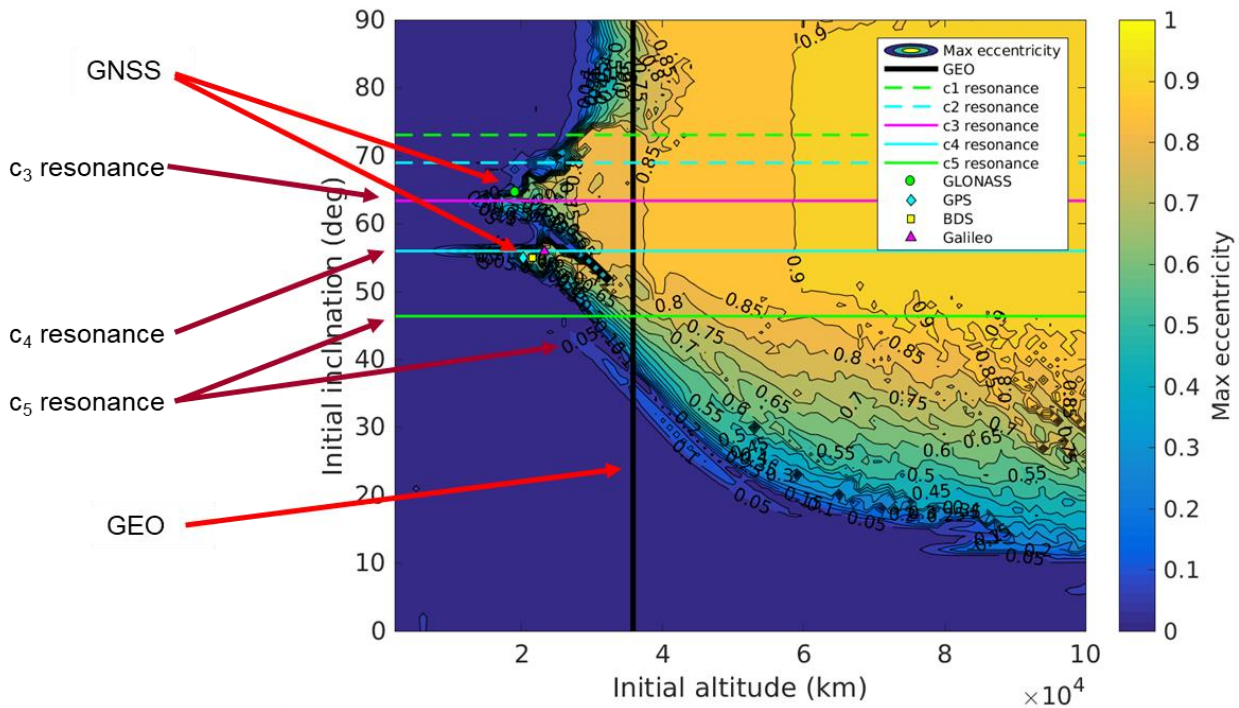


Figure 6. 2D Plot of maximum eccentricity over 200 years vs. initial altitude and inclination, initial RAAN = 180°.

Fig. 7 is a 2D plot of orbital lifetime vs. initial inclination and altitude of the disposal orbit for initial RAAN = 180°. From this plot it is seen that the inclination has to be above 50° for the orbital lifetime to be less than 200 years. It is also seen from this plot that the GNSS near the c₄ resonance can in general achieve orbital lifetime less than 200 years. This is evident from the BeiDou System (BDS) point and the Galileo point. The situation for the GPS point is a little bit less clear on this plot, but previous

studies by the authors have shown that proper selection of initial RAAN and AOP can achieve GPS orbital lifetime less than 200 years. On the other hand, for GLONASS near the c₃ resonance, orbital lifetime less than 200 years is not achieved for the current altitude. That system does see high eccentricity growth, but the altitude is too low for the resonance to be strong enough to induce orbital reentry within 200 years.

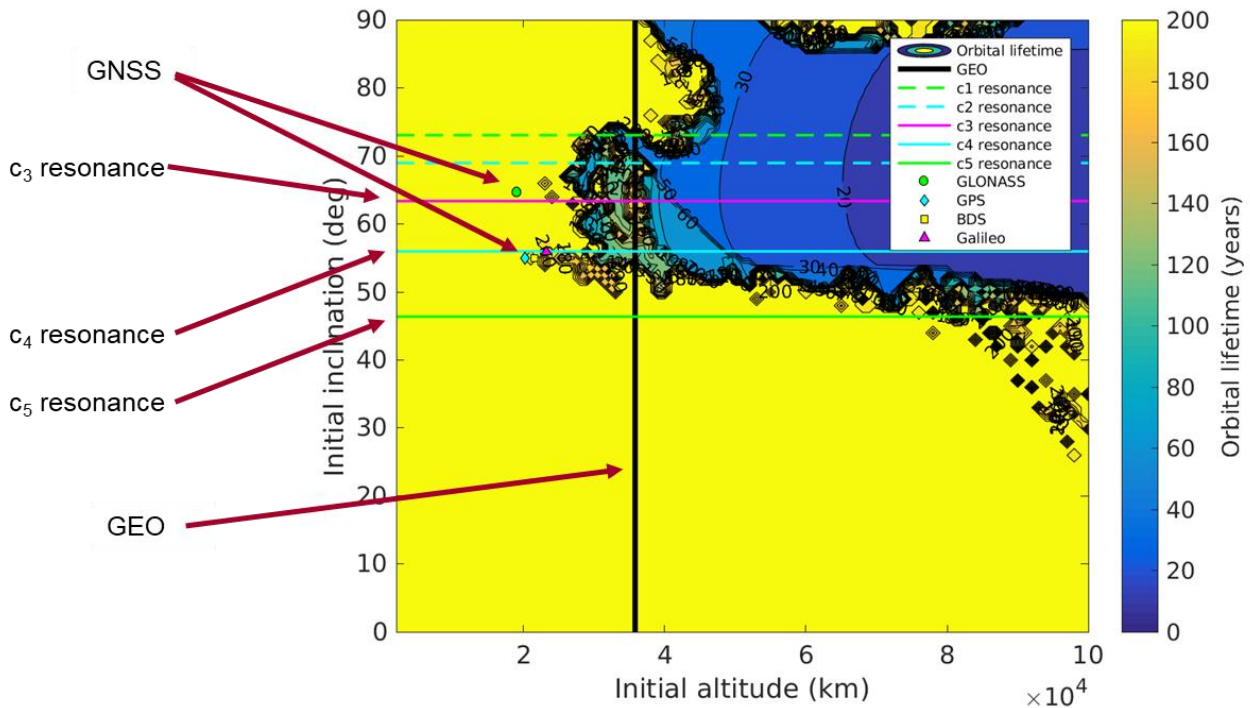


Figure 7. 2D Plot of orbital lifetime vs. initial altitude and inclination, initial RAAN = 180°.

6 COLLISION PROBABILITY ANALYSIS

A collision probability assessment was performed to quantify the risk reduction achieved by reducing orbital lifetime. The background population from the Aerospace Debris Environment Projection Tool (ADEPT) [17] was used for the analysis. An orbit trace crossing (OTC) method was used to compute collision probability. Fig. 8 illustrates an orbit trace crossing between two objects. For each pairing of objects, all crossings of the orbit traces (OTC events) over the assessment time interval are determined. The evolution of the orbit traces is accounted for by using the TRACE results for the spacecraft and background object orbital element files from ADEPT. The collision probability at each OTC event is computed assuming the in-track positions (mean anomalies) of the objects are uniformly distributed over 360°. The mean number of collisions is determined by summing collision probabilities from all OTC events in the assessment time interval. A description of this method and a comparison with a conjunction miss distance method are presented in [18]. These runs were executed on the Aerospace computing cluster.

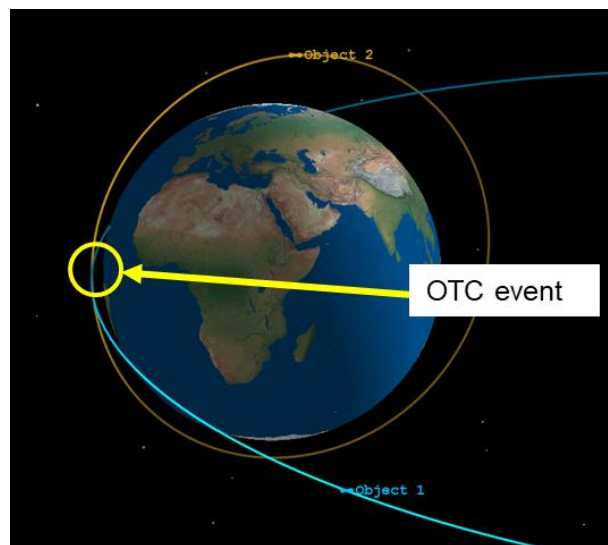


Figure 8. Illustration of an orbit trace crossing event between two objects (rendered with Satellite Orbit Analysis Program).

The collision radius for each object pair is required for the collision probability computation. The spacecraft mean contact radius was assumed to be 2.52 m (computed from the circular projected spacecraft area of 20 m²). Contact radii of the current background objects are part of the ADEPT model. For each object pair, the

mean collision radius is the sum of the mean contact radii of both objects.

ADEPT generates a model of the current and future Earth orbital background population. It includes orbit trajectories and sizes for each object. The following populations were used in this analysis.

- Catalog population: Objects from the unclassified two-line element set catalog of resident space objects.
- A future launch model (FLM) population.
- First generation debris from future collisions. There are 100 separate populations resulting from 100 Monte Carlo sets of future collisions. Probability of collision with the objects in this group are determined for each Monte Carlo debris population. Only the mean results over the 100 Monte Carlo debris populations are presented in this paper.

The catalog and FLM populations have a reference date of December 21, 2020. The future collisional debris population is from the version of ADEPT that has a reference date of June 6, 2017. Updating that population was beyond the scope of the study.

Trajectory files for all the objects were created using the mean element propagation code MEANPROP, which uses the Draper Semi-Analytic Orbit Propagation Theory. The force model settings were:

- 16x16 EGM-96 Earth gravity model.
- Sun and Moon gravity.
- Solar radiation pressure; assumed reflectivity coefficient = 1.3.
- MSISE-90 atmosphere model, with an assumed drag coefficient of 2.2. Monthly predictions of 50-percentile level of solar flux (F10.7) and geomagnetic index (A_p) from NASA Marshall Space Flight Center (based on NOAA data) from June 2017 to 2030 were used. For years after 2030, the last 11-years of MSFC predicted data were repeated into the future.

Only objects with a size greater than 10 cm (collision radius greater than 5 cm) are included in this collision probability analysis, in accordance with the 2019 ODMSP.

The FLM population consists of satellites, launch vehicle stages, and mission-related objects that are placed into Earth orbit in the future. The FLM objects are divided into several groups.

- Objects associated with continuously replenished constellations (CRC group).
- Objects associated with satellites in GEO orbits that control inclination to near zero.
- Objects associated with satellites in GEO orbits that allow inclination to drift.
- Remaining non-CRC objects (NONCRC group).

The CRCs are constantly replenished to maintain the full constellations. The CRC group models Iridium, Globalstar, Orbcomm, OneWeb, Starlink, O3b, GLONASS, GPS, the MEO component of the BeiDou navigation satellite system, and Galileo. The GEO population was generated by re-producing launches over the 15-year period prior to the simulation reference start date. The NONCRC population was generated by reproducing launches over the 10-year period prior to the simulation reference start date. An expected large increase in the number of CubeSats is not included in this study.

After mission operations were over, each FLM satellite was moved to a disposal orbit. A 100% post mission disposal (PMD) scenario was used in this analysis. In this scenario, all world-wide future launched objects are placed in disposal orbits that comply with the IADC Guidelines.

All future LEO satellites and upper stages are left on disposal orbits with lifetime less than or equal to 25 years or moved to a storage disposal orbit above LEO (perigee altitude greater than or equal to 2000 km). For objects that are moved to a disposal orbit with lifetime less than or equal to 25 years from a mission orbit that has an orbital lifetime exceeding 25 years, the orbital lifetime is reduced by lowering perigee to an altitude determined by an empirical formula derived from MEANPROP runs.

All future GEO satellites are left on storage disposal orbits above GEO. The GEO altitude boundary is determined according to the formula in the IADC Guidelines. In addition, eccentricity is set to 0.003.

Operational satellites are contained in the following groups.

- CRCs.
- GEO satellites that control inclination.
- GEO satellites that allow inclination to drift.
- Remaining satellites in the NONCRC group.

All of the remaining objects make up the inactive population.

Fig. 9 shows the results of the collision probability analysis. This 3D surface plot shows collision probability with inactive objects over 200 years on the z-axis and the color bar as a function of the initial inclination and altitude of the disposal orbit for initial RAAN = 180°. In this plot it is seen that there is a peak at the GNSS altitude region and a peak at the GEO altitude region. At the high

inclination and altitude range, collision probability is lowest in the same region where orbital lifetime is less than 200 years. At low inclinations there is a region of low collision probability well above GEO where eccentricity growth is low and the background population is sparse.

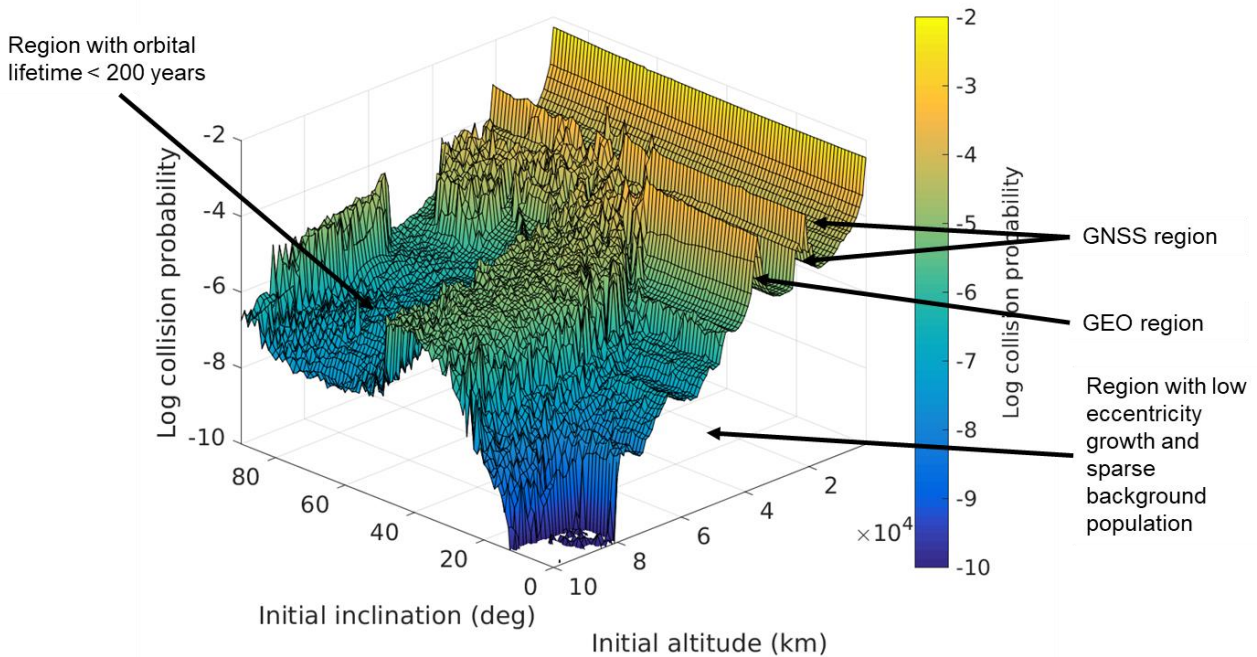


Figure 9. 3D Plot of collision probability vs. initial altitude and inclination, initial RAAN = 180°.

Fig. 10 is a 2D version of Fig. 9. Three distinct regions can be seen here.

1. A region in the high inclination range above 50° and altitude range starting in the GNSS region and extending upward (including inclined GEO orbits) with low collision probability because of reentry within 200 years.
2. A region in the low inclination range below 20° and altitude range above 47,000 km with low collision probability. This region corresponds to the region where eccentricity growth is low, but it starts at higher altitude where the background population is sparse.

3. A region in the middle, which has higher collision probability because the eccentricity growth is significant enough to cause spreading down to altitudes where there are more background objects, but not high enough to result in reentry within 200 years.

It is also seen that the GNSS are in regions with slightly darker color, indicating that the collision probability is lower due to eccentricity growth. For GEO, the variation of the collision probability cannot be accurately inferred because this sweep was too coarse. The SMA altitude increment was 1,000 km, whereas the GEO region has a sharp peak in the 200 km range above the 36,000 km altitude range, essentially due to the GEO graveyard.

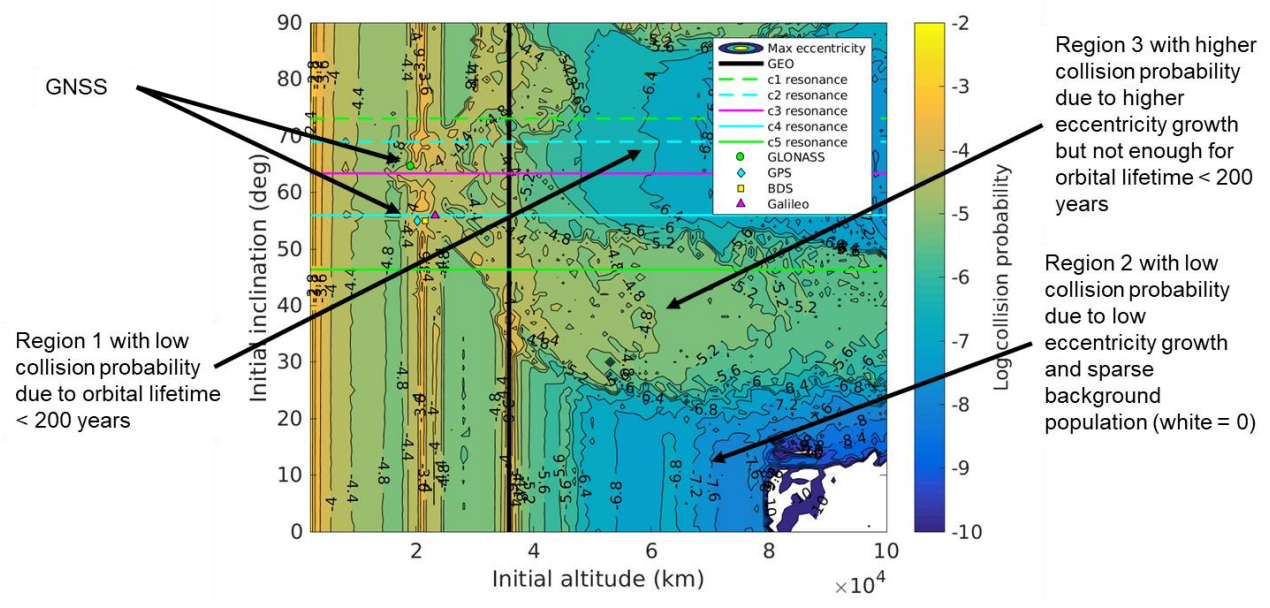


Figure 10. 2D Plot of collision probability vs. initial altitude and inclination, initial RAAN = 180° .

7 CONCLUSIONS

The study results show that orbital lifetime less than 200 years can be achieved for a broad altitude and inclination region. In general, that inclination must be above 50° to achieve orbital lifetime less than 200 years. This region includes inclined GEO orbits. At the lower end of this altitude range, distinct inclination ranges corresponding to the c_3 and c_4 resonances can achieve orbital lifetime less than 200 years, and this is therefore applicable to the GPS, BDS, and Galileo systems. Unfortunately, the current altitude of GLONASS is too low to achieve orbital lifetime less than 200 years. Collision probability is lowest in the inclination/altitude range where orbital lifetime is less than 200 years, or in the low inclination range below 20° and high-altitude range above 47,000 km, where disposal orbits are stable and the background population is sparse.

8 ACKNOWLEDGMENTS

This work reflects research conducted under U.S. Air Force Space and Missile Systems Center Contract FA8802-09-C-0001. The authors wish to thank several individuals and organizations for their support of this work and assistance in preparing this paper. Technical committee members Ragini Joshi, David Emmert, and Chelsea Thangavelu, as well as George Pollock, provided technical review of the paper. The Aerospace Technical Investment Program provided support for this work. The Aerospace Corporation's Office of Technical Relations provided publication clearance review.

9 REFERENCES

1. U.S. Government Orbital Debris Mitigation Standard Practices, 2019, https://orbitaldebris.jsc.nasa.gov/library/usg_orbital_debris_mitigation_standard_practices_november_2019.pdf.
2. Jenkin, A.M., McVey, J.P., Sorge, M.E., "Orbital Lifetime and Collision Risk Reduction for Inclined Geosynchronous Disposal Orbits," *Acta Astronautical*, Volume 161, August 2019, pp. 153-165.
3. Jenkin, A.B., McVey, J.P., Sorge, M.E., "Assessment of Time Spent in the LEO, GEO, and Semi-Synchronous Zones by Spacecraft on Long-Term Reentering Disposal Orbits," Paper No. IAC-20-A6.4.6,x57316, 71st International Astronautical Congress (IAC), The CyberSpace Edition, October 12-14, 2020.
4. Colombo, C., Gkolias, I., "Analysis of the Orbit Stability in the Geosynchronous Region for End-of-Life Disposal," Proceedings of the Seventh

European Conference on Space Debris, Darmstadt, Germany, April 18-21, 2017.

5. Gkolias, I., Colombo, C., "Disposal Design for Geosynchronous Satellites Revisited," Paper No. AAS 18-376, AAS/AIAA Astroynamics Specialists Conference, Snowbird, UT, August 20-23, 2018.
6. Jenkin, A.B., McVey, J.P., Emmert, D.E., Sorge, M.E., "Comparison of Disposal Options for Tundra Orbits in Terms of Delta-V Cost and Long-Term Collision Risk," *Journal of Space Safety Engineering*, December 29, 2020, <https://reader.elsevier.com/reader/sd/pii/S2468896720301464?token=504F43E0147EB0358C4624688714F3598A9661FCB4094757868F5D21C677C6A1990E234E2AC2C6F56D8ADD0F23970750>.
7. Skoulidou, D.K., Rosengren, A.J., Tsiganis, K., Voyatzis, G., "Cartographic Study of the MEO Phase Space for Passive Debris Removal," Proceedings of the Seventh European Conference on Space Debris, Darmstadt, Germany, April 18-21, 2017.
8. Skoulidou D.K., A.J. Rosengren, K. Tsiganis and G. Voyatzis, "Medium Earth Orbit dynamical survey and it use in passive debris removal", *Adv. Sp. Res.* 63, p. 3646-3674, 2018.
9. Colombo, C., et al., de Miguel, G.V., Skoulidou, D.K., Banos, N.M., Alessi, E.M., Gkolias, I., Carzana, L., Letterio, F., Schettino, G., Tsiganis, K., Rossi, A., "ReDSHIFT Disposal Module for the Design of End-of-Life Disposal Trajectories for LEO to GEO Missions," Paper No. IAC-19,A6,6,4, 70th International Astronautical Congress, Washington, D.C., October 21-25, 2019.
10. Chao, C.C., Hoots, F.R., *Applied Orbit Perturbation and Maintenance*, The Aerospace Press, El Segundo, CA, AIAA, Reston, VA, 2018, 2nd Edition.
11. Chao, C.C., *Applied Orbit Perturbation and Maintenance*, The Aerospace Press, El Segundo, CA, AIAA, Reston, VA, 2005, 1st Edition.
12. Vallado, D.A., *Fundamentals of Astrodynamics and Applications*, McGraw-Hill, 1997.
13. Lidov, M.L., "The Evolution of the Orbits of Artificial Satellites of Planets under the Action of Gravitational Perturbations of External Bodies," *Planet. Space Sci.*, 1962, Vol. 9, pp. 719 to 759.
14. Kozai, Y., "Secular Perturbations of Asteroids with High Inclination and Eccentricity," *The Astronomical Journal*, Vol. 67, No. 9, November 1962.

15. Gkolias, I., Daquin, J., Gachet, F., Rosengren, A.J., "From Order to Chaos in Earth Satellite Orbits," *The Astronomical Journal*, 152:119, 2016 November.
16. Laplace Plane,
https://en.wikipedia.org/wiki/Laplace_plane.
17. Jenkin, A.B., Sorge, M.E., Peterson, G.E., McVey, J.P., "Recent Enhancements to ADEPT and Sample Debris Environment Projections," Paper No. IAC-15.A6.2.2, 66th International Astronautical Congress, Jerusalem, Israel, October 12-16, 2015.
18. Jenkin, A.B., McVey, J.P., "Constellation and 'Graveyard' Collision Risk for Several MEO Disposal Strategies," Proceedings of the Fifth European Conference on Space Debris, Darmstadt, Germany, March 30-April 2, 2009 (ESA SP-672, July 2009).